Electronic Supplementary Material (ESI) for Dalton Transactions.

Supporting Information: Stabilization of Ammonium Borohydride in Solid Solutions of NH_4BH_4-MBH_4 (M = K, Rb, Cs)

Jakob B. Grinderslev*, Torben R. Jensen*

[a]*Interdisciplinary Nanoscience Center (iNANO) and Department of Chemistry, Aarhus University, Langelandsgade 140, DK-8000 Aarhus C, Denmark*

*Corresponding authors: Dr. Jakob B. Grinderslev (jakobg@inano.au.dk) and Prof. Torben R. Jensen (trj@chem.au.dk)

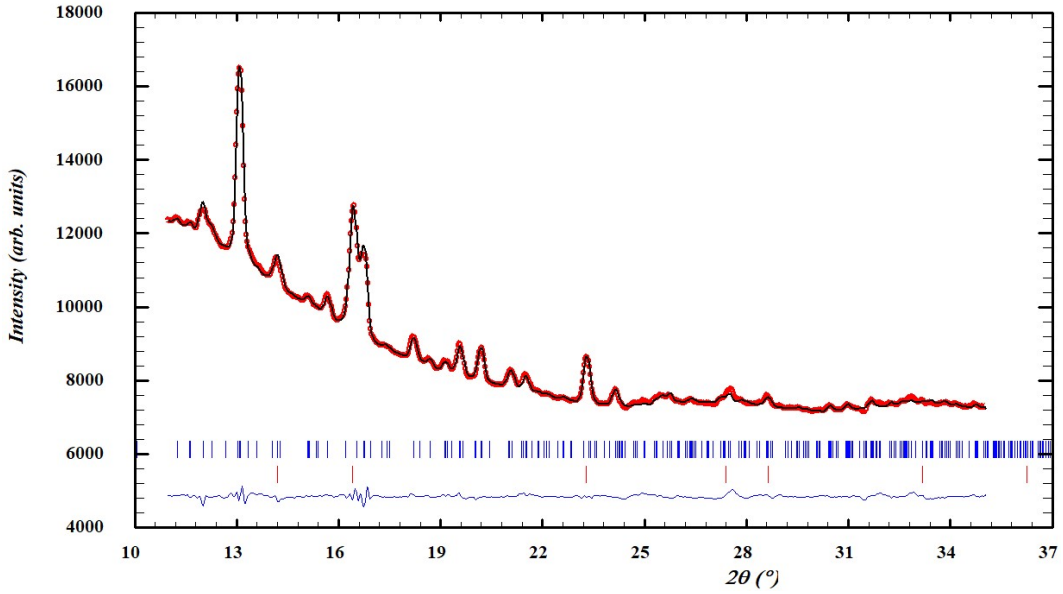

Figure S1. Rietveld refinement of SR PXD data of cryomilled NH_4BH_4, measured at T = 0 °C, λ = 0.9938 Å, showing experimental (red circles) and calculated (black line) PXD patterns, and a difference plot below (blue line). Tick marks: (blue) *ortho*-$[(NH_3)_2BH_2]BH_4$ (74 wt%), (red) NH_4BH_4 (26 wt%). Final discrepancy factors: R_p = 0.378 %, R_{wp} = 0.540 % (not corrected for background), R_p = 12.6 %, R_{wp} = 10.5 % (Conventional Rietveld R-factors), R_{Bragg}(*ortho*-$[(NH_3)_2BH_2]BH_4$) = 9.29 %, $R_{Bragg}(NH_4BH_4)$ = 1.95 % and global χ^2 = 73.2

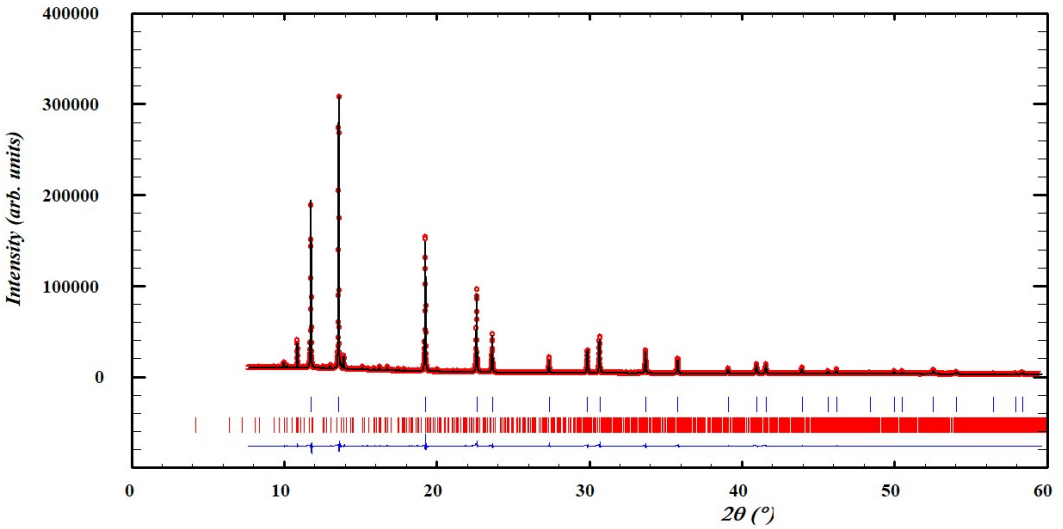

Figure S2. Rietveld refinement of SR PXD data of Rb31 measured at T = -21 °C, λ = 0.825775 Å, showing experimental (red circles) and calculated (black line) PXD patterns, and a difference plot below (blue line). Tick marks: (blue) $(NH_4)_{0.52}Rb_{0.48}BH_4$ (77.4 wt%), (red) *ortho*-$[(NH_3)_2BH_2]BH_4$ (22.6 wt%). Final discrepancy factors: R_p = 2.18 %, R_{wp} = 3.38 % (not corrected for background), R_p = 10.4 %, R_{wp} = 8.66 % (Conventional Rietveld R-factors), $R_{Bragg}((NH_4)_{0.54}Rb_{0.46}BH_4)$ = 2.33 %, $R_{Bragg}([(NH_3)_2BH_2]BH_4)$ = 19.4 % and global χ^2 = 68.0

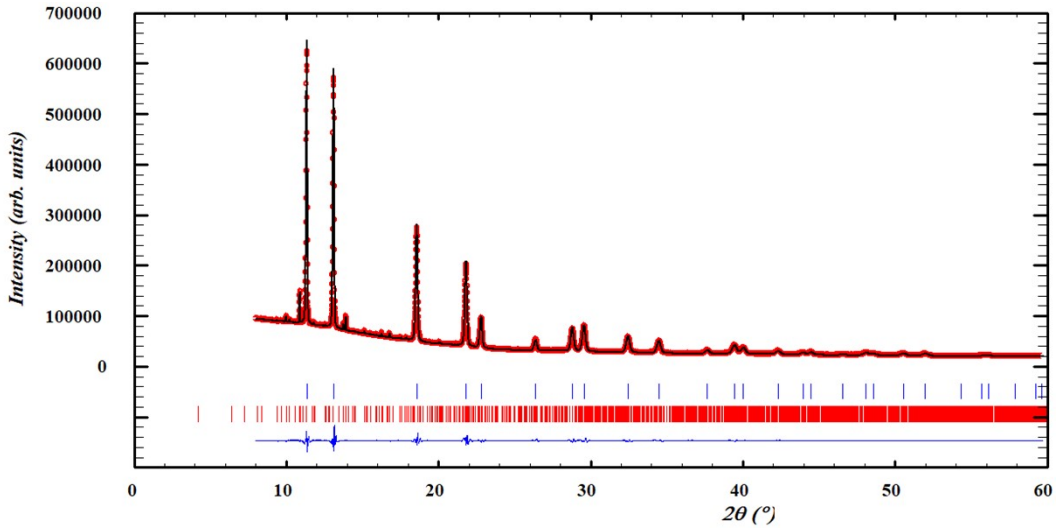

Figure S3. Rietveld refinement of SR PXD data of Cs31 measured at T = -22 °C, λ = 0.82646 Å, showing experimental (red circles) and calculated (black line) PXD patterns, and a difference plot below (blue line). Tick marks: (blue) $(NH_4)_{0.45}Cs_{0.55}BH_4$ (79.3 wt%), (red) *ortho*-$[(NH_3)_2BH_2]BH_4$ (20.7 wt%). Final discrepancy factors: R_p = 1.11 %, R_{wp} = 1.78 % (not corrected for background), R_p = 7.71 %, R_{wp} = 6.22 % (Conventional Rietveld R-factors), $R_{Bragg}((NH_4)_{0.45}Cs_{0.55}BH_4)$ = 0.864 %, $R_{Bragg}([(NH_3)_2BH_2]BH_4)$ = 11.2 % and global χ^2 = 14.7

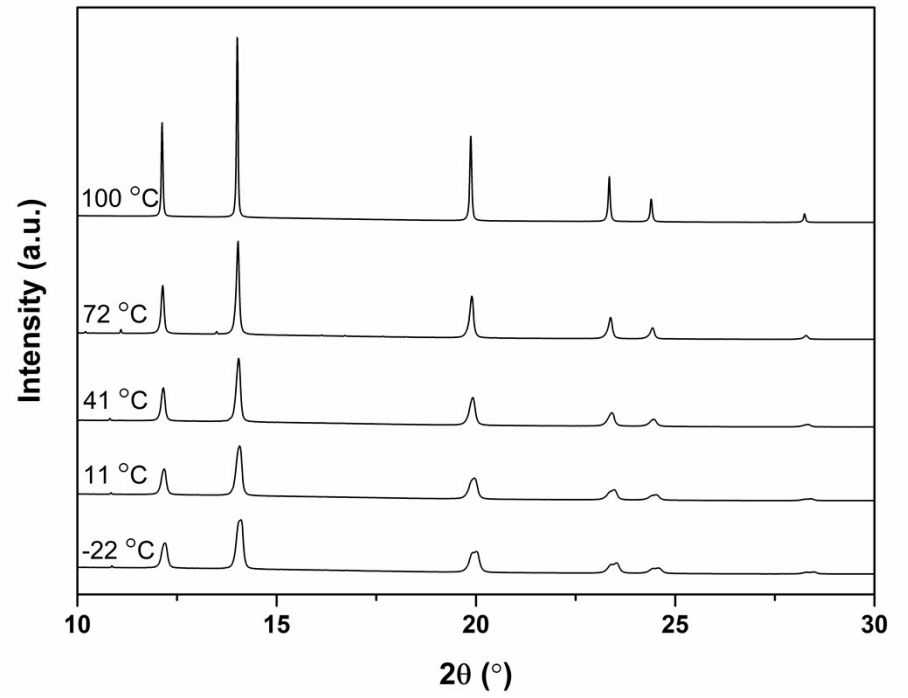

Figure S4. Selected SR PXD data of K13 heated from T = -22 to 100 °C ($\Delta T/\Delta t$ = 5 °C/min, p(Ar) = 1 bar, λ = 0.825775 Å). The two solid solutions merge upon heating.

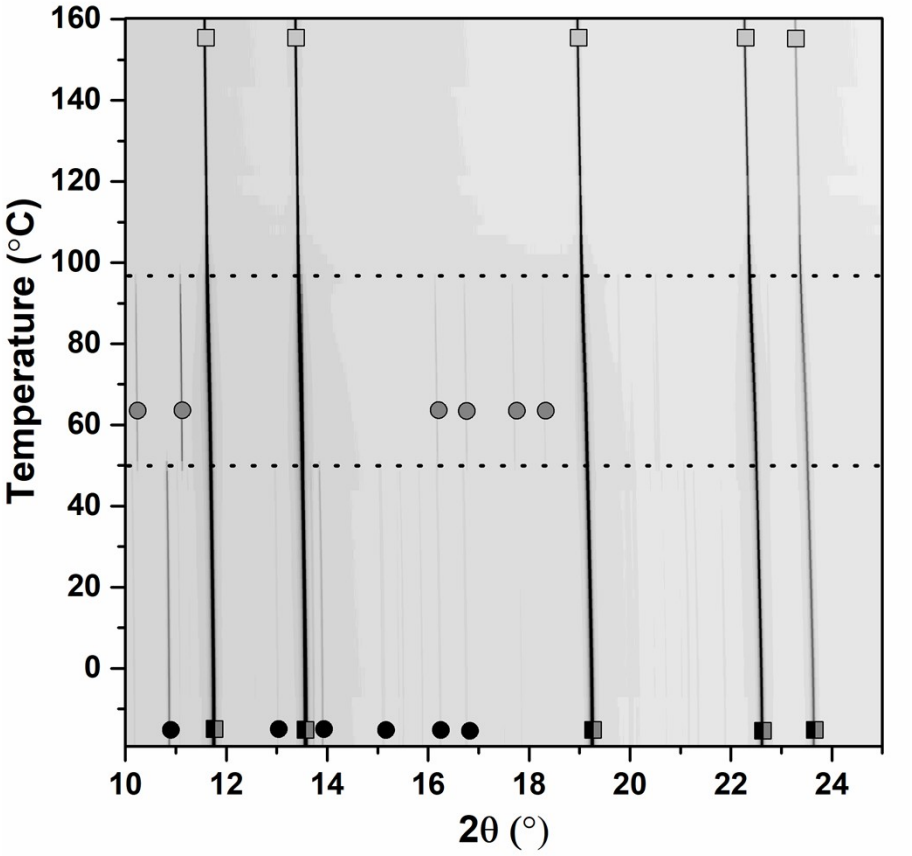

Figure S5. *In situ* SR PXD of Rb31 at Diamond, heated from T = -20 to 160 °C ($\Delta T/\Delta t$ = 5 °C/min, p(Ar) = 1 bar, λ = 0.82646 Å). Symbols: Black circle: *ortho*-$[(NH_3)_2BH_2]BH_4$, grey circle: *tetra*-$[(NH_3)_2BH_2]BH_4$, grey/black square: $(NH_4)_xRb_{1-x}BH_4$, grey square: $RbBH_4$. The dotted lines show the polymorphic transition from *ortho*- to *tetra*-$[(NH_3)_2BH_2]BH_4$ (T ~ 48 °C) and the decomposition of *tetra*-$[(NH_3)_2BH_2]BH_4$ (T ~ 96 °C).

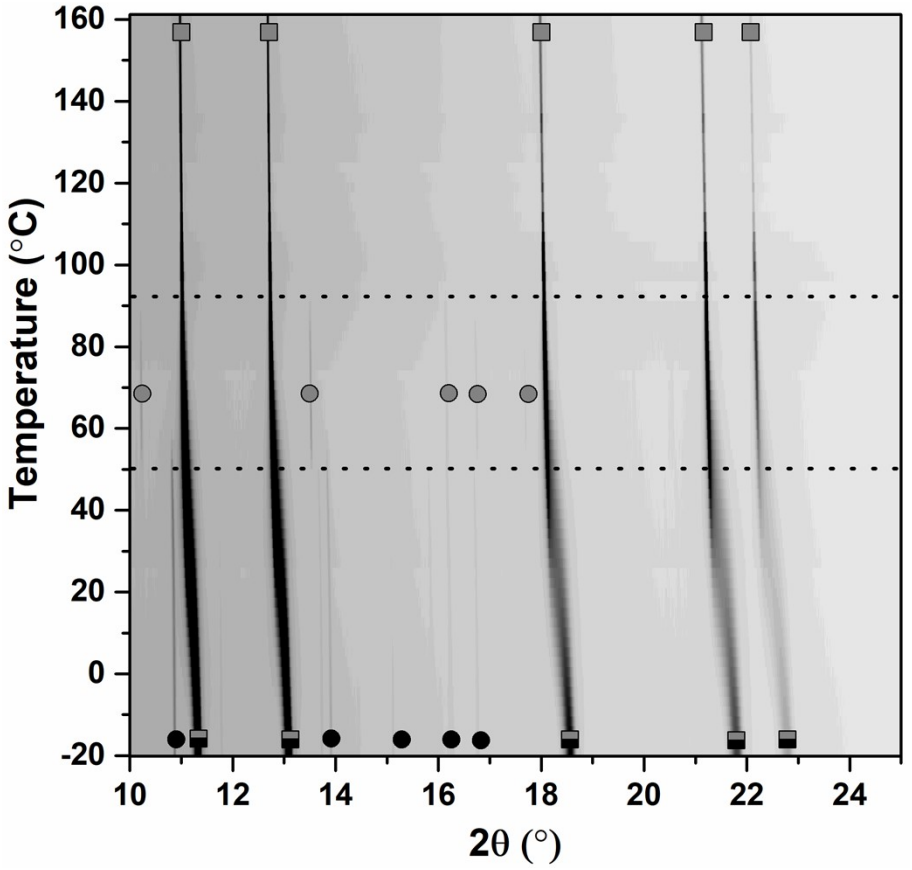

Figure S6. *In situ* SR PXD of Cs31 at Diamond, heated from T = -20 to 160 °C ($\Delta T/\Delta t$ = 5 °C/min, p(Ar) = 1 bar, λ = 0.82646 Å). Symbols: Black circle: *ortho*-$[(NH_3)_2BH_2]BH_4$, grey circle: *tetra*-$[(NH_3)_2BH_2]BH_4$, grey/black square: $(NH_4)_xCs_{1-x}BH_4$, grey square: $CsBH_4$. The dotted lines show the polymorphic transition from *ortho*- to *tetra*-$[(NH_3)_2BH_2]BH_4$ (T ~ 48 °C) and the decomposition of *tetra*-$[(NH_3)_2BH_2]BH_4$ (T ~ 96 °C).

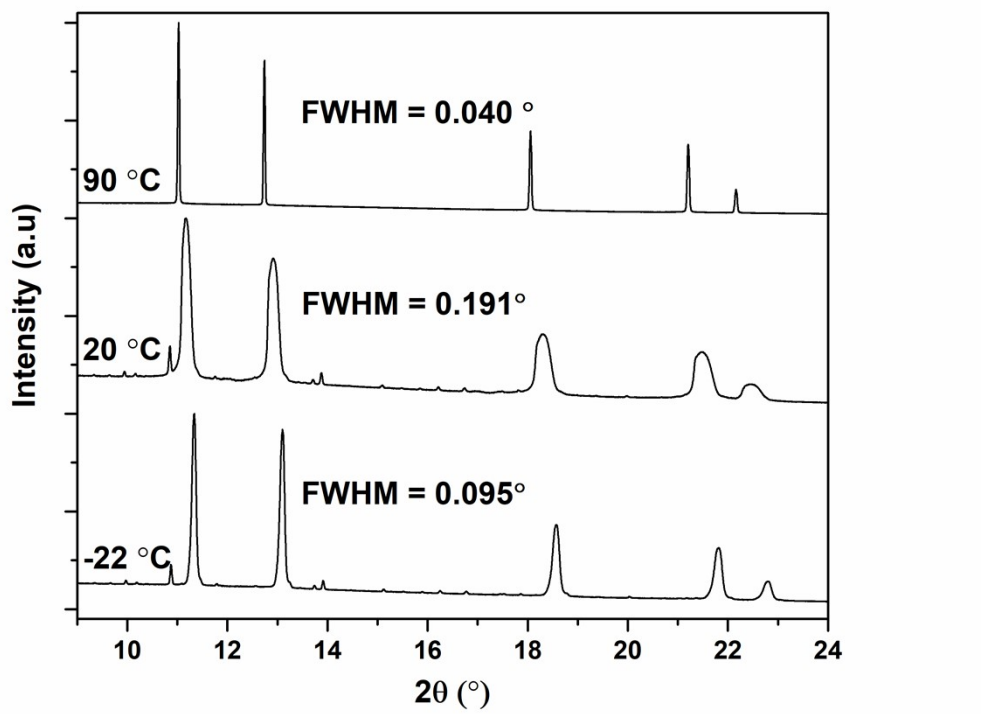

Figure S7. SR PXD and FWHM values of Cs31 at T = -22 °C, 20 °C and 90 °C, λ = 0.82646 Å.

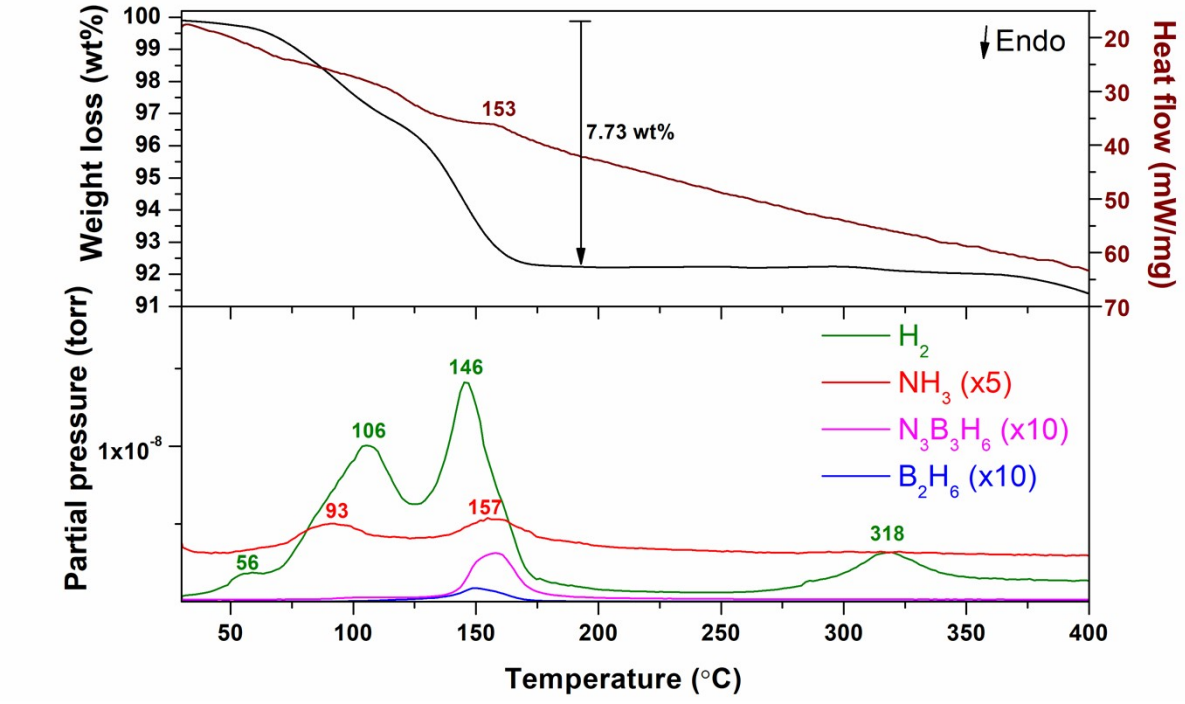

Figure S8. TG-DSC-MS of Rb11 in the temperature range T = 30 to 400 °C ($\Delta T/\Delta t$ = 5 °C/min).

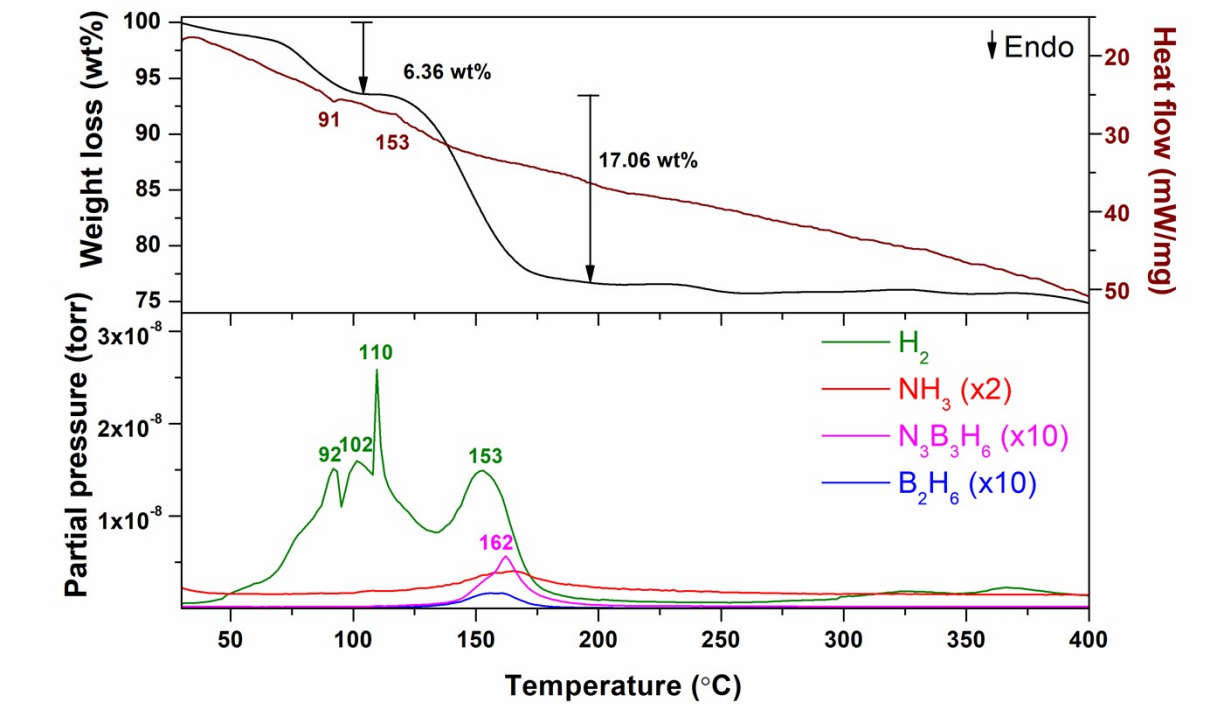

Figure S9. TG-DSC-MS of Rb31 in the temperature range T = 30 to 400 °C ($\Delta T/\Delta t$ = 5 °C/min).

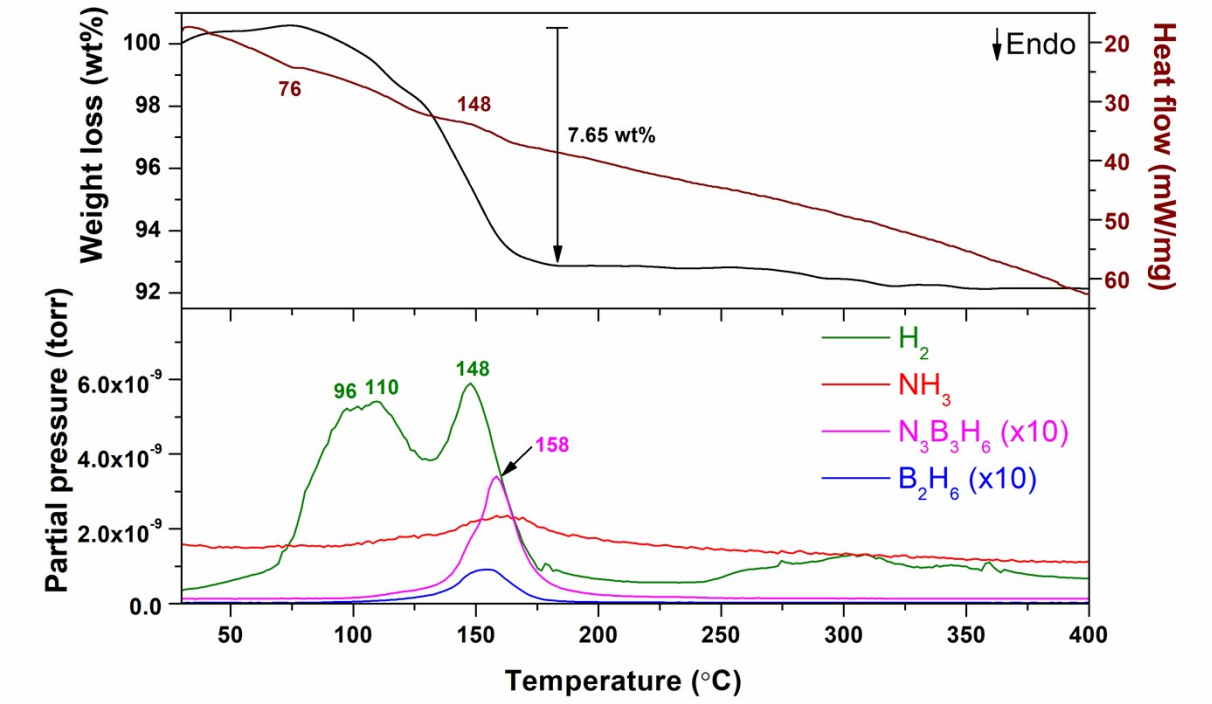

Figure S10. TG-DSC-MS of Cs11 in the temperature range T = 30 to 400 °C ($\Delta T/\Delta t$ = 5 °C/min).

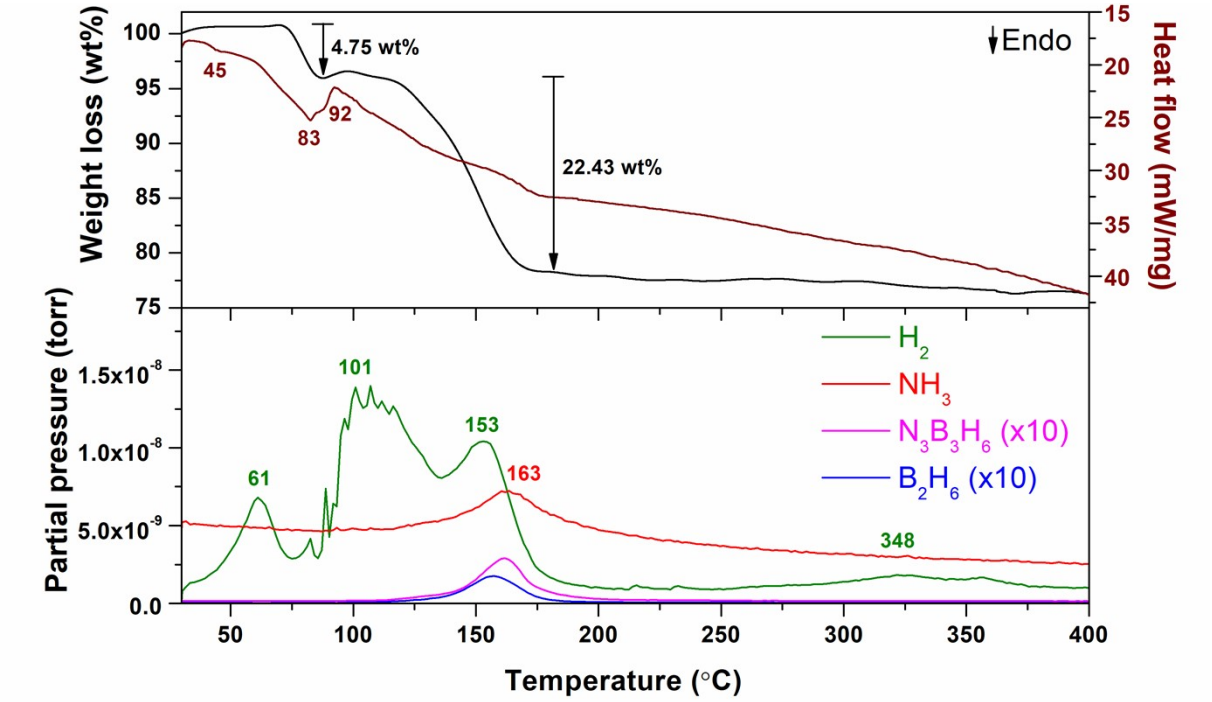

Figure S11. TG-DSC-MS of Cs31 in the temperature range T = 30 to 400 °C ($\Delta T/\Delta t$ = 5 °C/min).